

## ELECTRONIC SUPPLEMENTARY INFORMATION

### **‘Kick-in the head’: High-performance and air-stable mononuclear Dy<sup>III</sup> single-molecule magnets with *pseudo-D*<sub>6h</sub> symmetry from an [1+1] Schiff-base macrocycle approach**

Alexandros S. Armenis,<sup>a</sup> Arpan Mondal,<sup>b</sup> Sean R. Giblin,<sup>c</sup> Dimitris I. Alexandropoulos,<sup>a</sup> Jinkui Tang,<sup>d</sup> Richard A. Layfield\*<sup>b</sup> and Theocharis C. Stamatatos\*<sup>a</sup>

<sup>a</sup> Department of Chemistry, University of Patras, Patras 26504, Greece. E-mail: thstama@upatras.gr; tel.: +30-2610996730.

<sup>b</sup> Department of Chemistry, School of Life Sciences, University of Sussex, Brighton BN1 9QR, U.K. E-mail: R.Layfield@sussex.ac.uk

<sup>c</sup> School of Physics and Astronomy, Cardiff University, Cardiff CF24 3AA, U.K.

<sup>d</sup> State Key Laboratory of Rare Earth Resource Utilization, Changchun Institute of Applied Chemistry, Chinese Academy of Sciences, Changchun 130022, P. R. China.

## 1. Materials and Physical Measurements

All experiments were carried out under aerobic conditions using materials and solvents as received without further purification. The organic precursor 2,9-diacarboxaldehyde-1,10-phenanthroline was synthesized as reported previously.<sup>1</sup> Infrared spectra were recorded in the solid state on a Bruker FT-IR spectrometer (ALPHA's Platinum ATR single reflection) in the 4000-400 cm<sup>-1</sup> range. Elemental analyses (C, H, N) were performed by the University of Patras microanalytical service. Powder X-ray diffraction (p-XRD) measurements were conducted on a Bruker D8 Advance X-ray diffractometer using Cu-K $\alpha$  radiation. Thermogravimetric analyses (TGA) were recorded on a Discovery TGA 55 instrument in the temperature range of 25-800 °C with a heating rate of 4 °C min<sup>-1</sup> under N<sub>2</sub> conditions. Direct current (dc) and alternating current (ac) magnetic susceptibility measurements were performed using a Quantum Design MPMS-XL7 and a Quantum Design MPMS3 SQUID (up to frequencies of 1 kHz) magnetometers, respectively. Ac susceptibility measurements up to 10 kHz were performed using a bespoke coil set integrated into the bore of a Quantum Design PPMS. Samples were prepared by gently crushing the crystalline materials before transferring them to a 7 mm NMR tube and covering them in eicosane. Then the tubes were flame-sealed under a static vacuum. The eicosane was melted in a water bath at 40 °C to prevent crystallite torquing. Diamagnetic corrections were applied using Pascal's constants.<sup>2</sup>

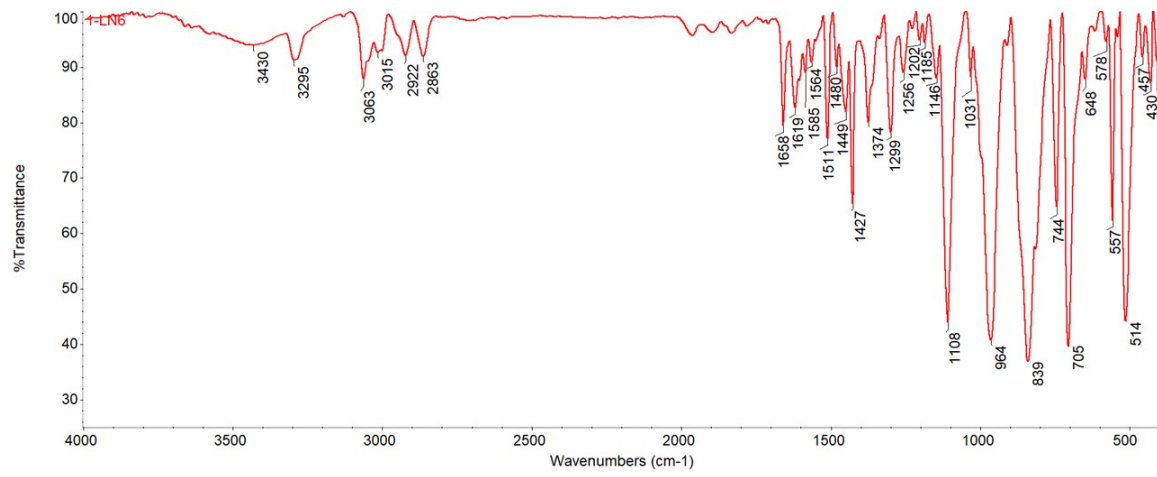
## 2. Synthesis, Structural and Spectroscopic Characterization

**Synthesis of [Dy(L<sub>phen</sub><sup>N6</sup>)(Ph<sub>3</sub>SiO)<sub>2</sub>](PF<sub>6</sub>) (1-L<sub>phen</sub><sup>N6</sup>):** 1,10-phenanthroline-2,9-dicarbaldehyde (0.20 mmol, 0.047 g), triethylenetetramine (0.20 mmol, 0.030 g), and DyCl<sub>3</sub>·6H<sub>2</sub>O (0.20 mmol, 0.075 g) were transferred to a round bottom flask containing 15 mL of methanol resulting in an orange clear solution. The mixture was refluxed for 24 hours giving an orange-yellow clear solution and then the solvent was removed under reduced pressure yielding an orange-yellow oil. To the oily residue was added a CH<sub>2</sub>Cl<sub>2</sub> solution (15 mL) containing Ph<sub>3</sub>SiOH (0.80 mmol, 0.222 g) and Et<sub>3</sub>N (0.80 mmol, 0.112 mL), and subsequently an aqueous solution (15 mL) of NH<sub>4</sub>PF<sub>6</sub> (0.20 mmol, 0.032 g), thus creating two layers. The reaction mixture was refluxed for 1 hour, and the orange-yellow

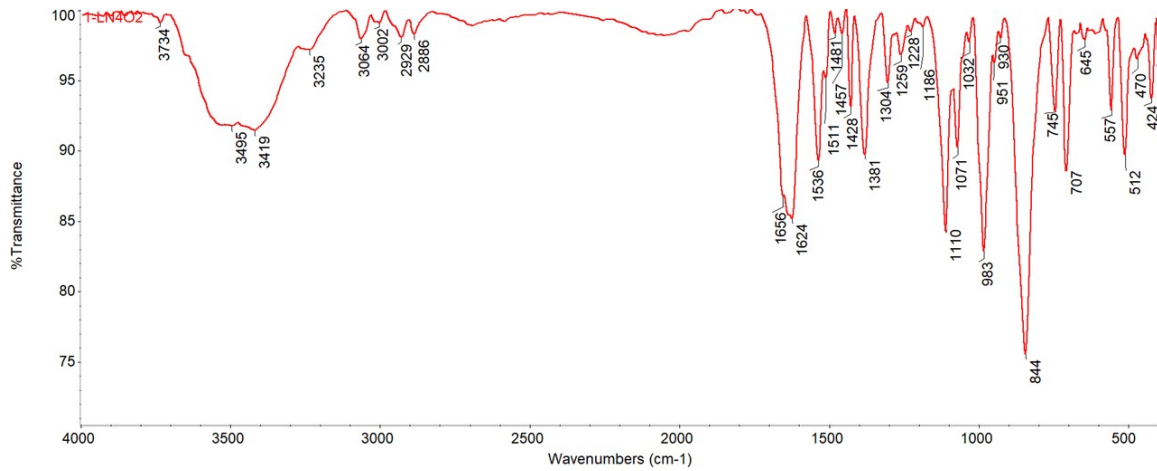
$\text{CH}_2\text{Cl}_2$  phase was separated with a separating funnel and then filtered, giving a clear yellow solution. Pale yellow plate-like crystals suitable for single-crystal X-ray diffraction were isolated after 2-3 days by layering the  $\text{CH}_2\text{Cl}_2$  solution with n-pentane. The crystals were collected by filtration, washed with  $\text{CH}_2\text{Cl}_2$  ( $2 \times 2$  mL), and dried in air. The yield was 42% (based on Dy). The air-dried solid was analyzed as  $\mathbf{1-L}_{\text{phen}}^{\text{N}6}$ . Anal. Calcd for  $\text{C}_{56}\text{H}_{52}\text{DyF}_6\text{N}_6\text{O}_2\text{PSi}_2$ : C, 55.83; H, 4.35; N, 6.98. Found: C, 55.91; H, 4.39; N, 6.90.

**Synthesis of  $[\text{Dy}(\text{L}_{\text{phen}}^{\text{N}4\text{O}2})(\text{Ph}_3\text{SiO})_2](\text{PF}_6)$  ( $\mathbf{1-L}_{\text{phen}}^{\text{N}4\text{O}2}$ ):** 1,10-phenanthroline-2,9-dicarbaldehyde (0.20 mmol, 0.032 g), 1,2-bis(2-aminoethoxy)ethane (0.20 mmol, 0.030 mL), and  $\text{DyCl}_3 \cdot 6\text{H}_2\text{O}$  (0.20 mmol, 0.075 g) were transferred to a round bottom flask containing 15 mL of methanol resulting in an orange clear solution. The mixture was refluxed for 24 hours giving a dark orange clear solution and then the solvent was removed under reduced pressure yielding an orange oily precipitate. To the residue was added a  $\text{CH}_2\text{Cl}_2$  solution (15 mL) containing  $\text{Ph}_3\text{SiOH}$  (0.80 mmol, 0.222 g) and  $\text{Et}_3\text{N}$  (0.80 mmol, 0.112 mL), and subsequently an aqueous solution (15 mL) of  $\text{NH}_4\text{PF}_6$  (0.20 mmol, 0.032 g), thus creating two layers. The reaction mixture was refluxed for 1 hour, and the orange-yellow  $\text{CH}_2\text{Cl}_2$  phase was separated with a separating funnel and then filtered, giving a clear yellow solution. Pale yellow plate-like crystals suitable for single-crystal X-ray diffraction were isolated after 2-3 days by layering the  $\text{CH}_2\text{Cl}_2$  solution with n-hexane. The crystals were collected by filtration, washed with  $\text{CH}_2\text{Cl}_2$  ( $2 \times 2$  mL), and dried in air. The yield was 36% (based on Dy). The air-dried solid was analyzed as  $\mathbf{1-L}_{\text{phen}}^{\text{N}4\text{O}2}$ . Anal. Calcd for  $\text{C}_{56}\text{H}_{50}\text{DyF}_6\text{N}_4\text{O}_4\text{PSi}_2$ : C, 55.74; H, 4.18; N, 4.64. Found: C, 55.81; H, 4.24; N, 4.57.

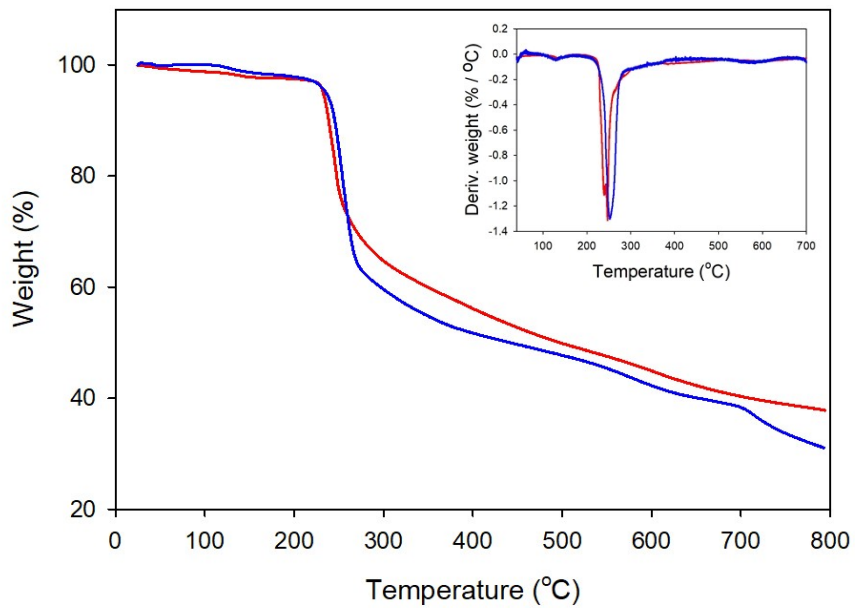
## Infrared Spectroscopy



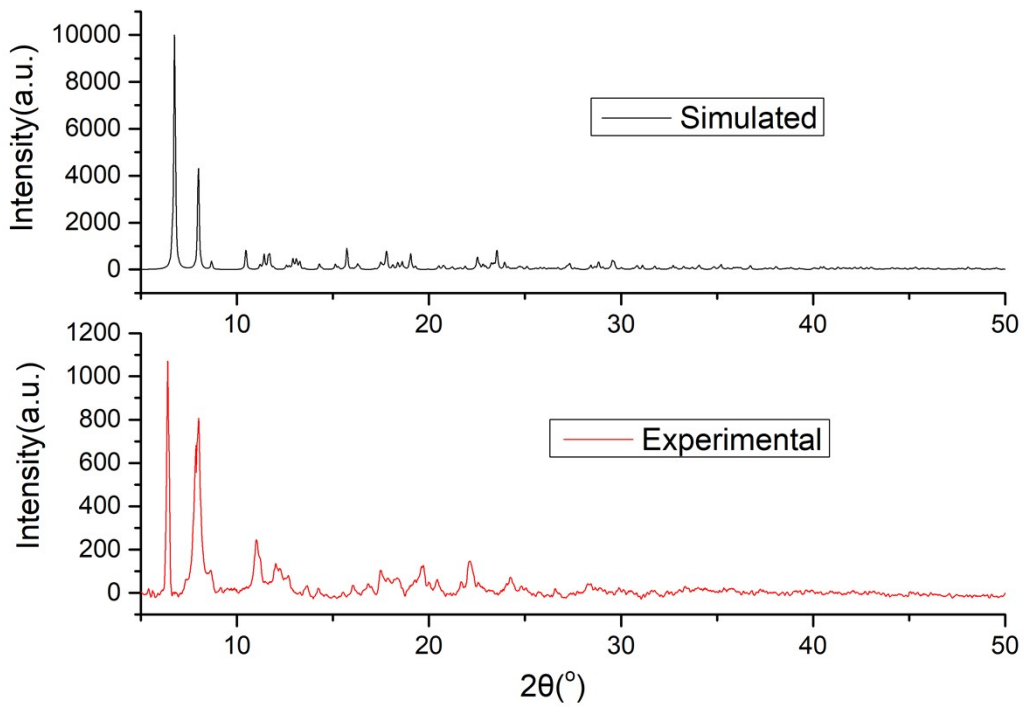
**Fig. S1** FT-IR spectra of complex  $1-\text{L}_{\text{phen}}^{\text{N}6}$ .



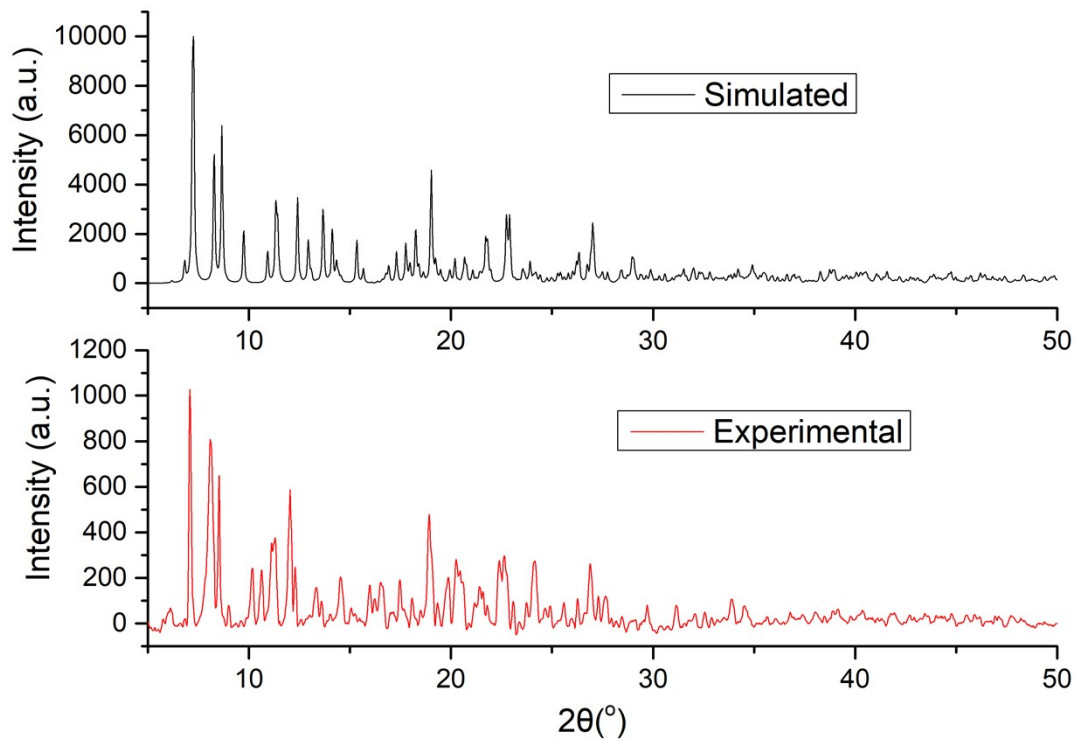
**Fig. S2** FT-IR spectra of complex  $1-\text{L}_{\text{phen}}^{\text{N}4\text{O}2}$ .



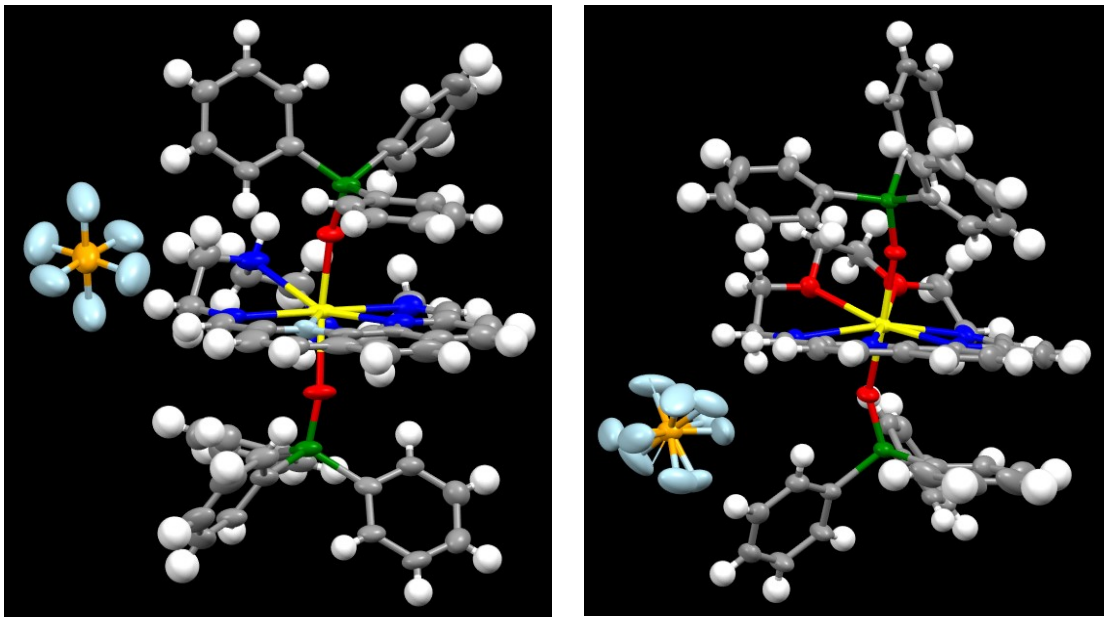
**Fig. S3** Thermogravimetric analyses of  $\mathbf{1}-\mathbf{L}_{\text{phen}}^{\text{N}6}$  (red line) and  $\mathbf{1}-\mathbf{L}_{\text{phen}}^{\text{N}4\text{O}2}$  (blue line).



**Fig. S4** Experimental and simulated powder X-ray diffraction (p-XRD) patterns of **1-L<sub>phen</sub><sup>N6</sup>**. The simulated pattern is calculated based on the structural model from the single-crystal X-ray diffraction data.



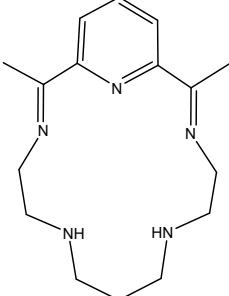
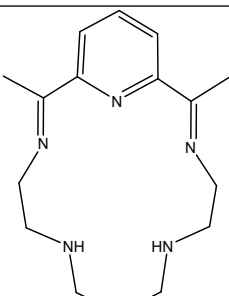
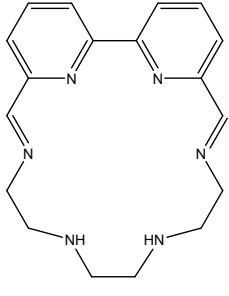
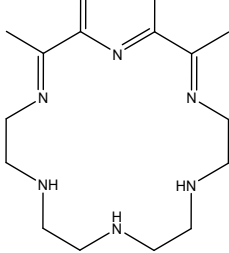
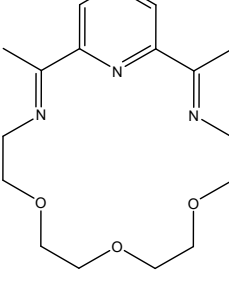
**Fig. S5** Experimental and simulated powder X-ray diffraction (p-XRD) patterns of **1-L<sub>phen</sub><sup>N4O2</sup>**. The simulated pattern is calculated based on the structural model from the single-crystal X-ray diffraction data.

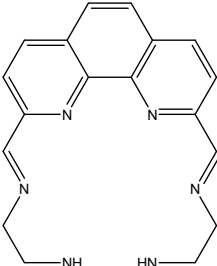
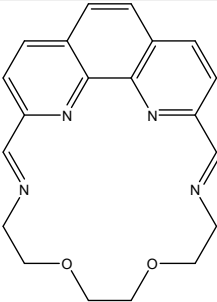


**Fig. S6** ORTEP representations of complexes  $\mathbf{1}-\mathbf{L}_{\text{phen}}^{\text{N}6}$  (left) and  $\mathbf{1}-\mathbf{L}_{\text{phen}}^{\text{N}4\text{O}2}$  (right); thermal ellipsoids are at the 30% probability level.

**Table S1.** All the previously reported mononuclear  $\text{Dy}^{\text{III}}$ , zero-field SMMs, containing [1+1] Schiff-base macrocycles.

Compound	Macrocyclic Structure	pseudo symmetry	$U_{\text{eff}} [\text{K}]$	Ref.
$[\text{Dy}(\mathbf{L}_1^{\text{N}5})(\text{Ph}_3\text{SiO})_2](\text{BPh}_4)$		$D_{5\text{h}}$	1108	[18c] main text
$[\text{Dy}(\mathbf{L}_2^{\text{N}5})(R/S-\text{BINOL})_2](\text{BPh}_4)$		$D_{5\text{h}}$	403(4)	[17d] main text

[Dy(L <sub>2</sub> <sup>N5</sup> )(Ph <sub>3</sub> SiO) <sub>2</sub> ](BPh <sub>4</sub> )		D <sub>5h</sub>	1085(45)	[18a] main text
[Dy <sub>0.05</sub> Y <sub>0.95</sub> (L <sub>2</sub> <sup>N5</sup> )(F <sub>2-</sub> PhO) <sub>2</sub> ](BPh <sub>4</sub> )		D <sub>5h</sub>	42(0.5)	[18b] main text
[Dy(L <sub>1</sub> <sup>N6</sup> )(Ph <sub>3</sub> SiO) <sub>2</sub> ](BPh <sub>4</sub> )		D <sub>6h</sub>	584(31)	[18d] main text
[Dy(L <sub>py</sub> <sup>N6</sup> )(Ph <sub>3</sub> SiO) <sub>2</sub> ](PF <sub>6</sub> ) <sup>*</sup> Two crystallographically independent molecules in the unit cell		D <sub>6h</sub> , C <sub>2v</sub> <sup>*</sup>	989(20)	[18e] main text
[Dy(L <sub>py</sub> <sup>N3O3</sup> )(Ph <sub>3</sub> SiO) <sub>2</sub> ](PF <sub>6</sub> )		D <sub>6h</sub>	1300(10)	[18e] main text

$[\text{Dy}(\text{L}_{\text{phen}}^{\text{N}6})(\text{Ph}_3\text{SiO})_2](\text{PF}_6)$		$D_{6h}$	790(54)	This work
$[\text{Dy}(\text{L}_{\text{phen}}^{\text{N}4\text{O}2})(\text{Ph}_3\text{SiO})_2](\text{PF}_6)$		$D_{6h}$	1360(21)	This work
Ligands' Abbreviations: $\text{L}_1^{\text{N}5}$ : (2E,14E)-2,15-dimethyl-3,7,10,14-tetraaza-1(2,6)-pyridinacyclopentadecaphane-2,14-diene; $\text{L}_2^{\text{N}5}$ : (2E,13E)-2,14-dimethyl-3,6,10,13-tetraaza-1(2,6)-pyridinacyclotetradecaphane-2,13-diene; $\text{L}_1^{\text{N}6}$ : (3E,13E)-4,7,10,13-tetraaza-1,2(2,6)-dipyridinacyclotetradecaphane-3,13-diene; $\text{L}_{\text{py}}^{\text{N}6}$ : (2E,15E)-2,16-dimethyl-3,6,9,12,15-pentaaza-1(2,6)-pyridinacyclohexadecaphane-2,15-diene; $\text{L}_{\text{py}}^{\text{N}3\text{O}3}$ : (2E,15E)-2,16-dimethyl-6,9,12-trioxa-3,15-diaza-1(2,6)-pyridinacyclohexadecaphane-2,15-diene; $\text{L}_{\text{phen}}^{\text{N}6}$ : (2E,12E)-3,6,9,12-tetraaza-1(2,9)-phenanthrolinacyclotridecaphe-2,12-diene; $\text{L}_{\text{phen}}^{\text{N}4\text{O}2}$ : (2E,12E)-6,9-dioxa-3,12-diaza-1(2,9)-phenanthrolinacyclotridecaphe-2,12-diene; $\text{Ph}_3\text{SiO}^-$ : triphenylsilanolate; R/S-BINOL: monodeprotonated R/S-1-(2-hydroxynaphthalen-2-ol); F <sub>2</sub> -PhO <sup>-</sup> : 3,5-difluorophenolate.				

## X-Ray Crystallographic details

Data were collected on a Rigaku XtaLAB Synergy-S single crystal X-ray diffractometer equipped with a CCD area detector and a graphite monochromator utilizing Cu K $\alpha$  radiation ( $\lambda = 1.54184 \text{ \AA}$ ). Selected pale yellow crystals of **1**- $\text{L}_{\text{phen}}^{\text{N}6}$  ( $0.314 \times 0.198 \times 0.079 \text{ mm}$ ) and **1**- $\text{L}_{\text{phen}}^{\text{N}4\text{O}2}$  ( $0.28 \times 0.15 \times 0.14 \text{ mm}$ ) were attached to glass fiber with paratone-N oil and transferred to a goniostat for data collection. Empirical absorption corrections (multiscan based on symmetry-related measurements) were applied using CrysAlis RED

software.<sup>3</sup> The structures were solved by direct methods using SIR92<sup>4</sup> and refined on  $F^2$  using SHELXL97,<sup>5</sup> SHELXL-2014/7,<sup>6</sup> and SHELXT.<sup>7</sup> Software packages used: CrysAlisCCD<sup>3</sup> for data collection, CrysAlisRED<sup>3</sup> for cell refinement and data reduction, WINGX for geometric calculations,<sup>8</sup> while MERCURY<sup>9</sup> and Diamond<sup>10</sup> were used for molecular graphics. For both compounds, the non-H atoms were treated anisotropically, whereas the H atoms were placed in calculated, ideal positions and refined as riding on their respective C atoms. Unit cell parameters and structure solution and refinement data for complexes **1-L<sub>phen</sub><sup>N6</sup>** and **1-L<sub>phen</sub><sup>N4O2</sup>** are listed in Table S2.

**Table S2.** Crystallographic data for compounds **1-L<sub>phen</sub><sup>N6</sup>** and **1-L<sub>phen</sub><sup>N4O2</sup>**.

Parameter	<b>1-L<sub>phen</sub><sup>N6</sup></b>	<b>1-L<sub>phen</sub><sup>N4O2</sup></b>
Formula	C <sub>56</sub> H <sub>52</sub> DyF <sub>6</sub> N <sub>6</sub> O <sub>2</sub> PSi <sub>2</sub>	C <sub>56</sub> H <sub>50</sub> DyF <sub>6</sub> N <sub>4</sub> O <sub>4</sub> PSi <sub>2</sub>
$F_w / \text{g}\cdot\text{mol}^{-1}$	1204.69	1206.69
Crystal system	Orthorhombic	Triclinic
Space group	$P2_12_12_1$	$\bar{P}1$
$a / \text{\AA}$	15.4944(1)	13.6004(4)
$b / \text{\AA}$	15.7789(1)	14.1007(4)
$c / \text{\AA}$	26.1724(3)	15.7213(4)
$\alpha / {}^\circ$	90.0	65.991(2)
$\beta / {}^\circ$	90.0	89.277(2)
$\gamma / {}^\circ$	90.0	73.563(2)
$V / \text{\AA}^3$	6398.75(9)	2623.41(13)
$Z$	4	2
$T / K$	293(2) K	190.1(5)
Radiation / $\lambda (\text{\AA})$	Cu K $\alpha$ / 1.54184	Cu K $\alpha$ / 1.54184
$\rho_{\text{calcd}} / \text{g cm}^{-3}$	1.251	1.467
Reflections collected/unique ( $R_{\text{int}}$ )	56998/13278 (0.0533)	36242/10691 (0.0324)
Reflections with $I > 2\sigma(I)$	12856	10437
No. of parameters	651	704
$R_1 [I > 2\sigma(I)], wR_2 [I > 2\sigma(I)]^{a,b}$	0.0613, 0.1687	0.0311, 0.0996

$R_1$ (all data), $wR_2$ (all data) <sup>a,b</sup>	0.0622, 0.1698	0.0317, 0.1003
$(\Delta/\sigma)_{\max}$	0.001	0.003
$\Delta\rho_{\max}/\Delta\rho_{\min}$ (e Å <sup>-3</sup> )	2.223/-1.317	0.935 /-0.803
CCDC number	2393281	2393282

<sup>a</sup>  $R_1 = \Sigma(|F_o| - |F_c|) / \Sigma(|F_o|)$ .

<sup>b</sup>  $wR_2 = \{\Sigma[w(F_o^2 - F_c^2)^2] / \Sigma[w(F_o^2)^2]\}^{1/2}$ ,  $w = 1 / [\sigma^2(F_o^2) + (aP)^2 + bP]$ , where  $P = [\max(F_o^2, 0) + 2 F_c^2] / 3$ .

**Table S3.** Selected bond distances (Å) and angles (°) for complex **1-L<sup>N6</sup><sub>phen</sub>**.

<b>Bond distances (Å)</b>	
Dy1-N1	2.558(8)
Dy1-N2	2.583(6)
Dy1-N3	2.569(7)
Dy1-N4	2.581(8)
Dy1-N5	2.684(6)
Dy1-N6	2.695(9)
Dy1-O1	2.159(5)
Dy1-O2	2.163(5)
<b>Bond angles (°)</b>	
O1-Dy1-O2	164.6(2)
N1-Dy1-N2	62.2(2)
N2-Dy1-N3	63.1(2)
N3-Dy1-N4	62.6(2)
N4-Dy1-N5	63.4(2)
N5-Dy1-N6	63.3(2)
N6-Dy1-N1	63.8(3)
O1-Dy1-N1	94.6(2)
O1-Dy1-N2	86.0(2)
O1-Dy1-N3	82.1(2)
O1-Dy1-N4	88.7(2)
O1-Dy1-N5	114.3(2)

O1-Dy1-N6	75.3(2)
O2-Dy1-N1	85.7(2)
O2-Dy1-N2	80.6(2)
O2-Dy1-N3	85.2(2)
O2-Dy1-N4	93.1(2)
O2-Dy1-N5	79.9(2)
O2-Dy1-N6	118.1(2)

**Table S4.** Selected bond distances ( $\text{\AA}$ ) and angles ( $^\circ$ ) for complex  $\mathbf{1}\cdot\text{L}_{\text{phen}}^{\text{N}4\text{O}2}$ .

<b>Bond distances (<math>\text{\AA}</math>)</b>	
Dy1-N1	2.570(2)
Dy1-N2	2.623(2)
Dy1-N3	2.628(2)
Dy1-N4	2.585(2)
Dy1-O1	2.602(2)
Dy1-O2	2.600(2)
Dy1-O3	2.142(2)
Dy1-O4	2.153(2)
<b>Bond angles (<math>^\circ</math>)</b>	
O3-Dy1-O4	174.52(7)
N3-Dy1-N2	61.15(7)
N2-Dy1-N1	61.77(7)
O2-Dy1-O1	59.18(7)
O1-Dy1-N4	60.92(6)
N4-Dy1-N3	60.94(7)
N1-Dy1-O2	61.07(7)
O3-Dy1-N3	83.35(7)
O3-Dy1-N2	83.65(7)
O3-Dy1-N1	96.44(7)
O3-Dy1-O2	83.37(7)

O3-Dy1-O1	85.56(7)
O3-Dy1-N4	99.22(7)
O4-Dy1-N3	101.62(7)
O4-Dy1-N4	81.41(7)
O4-Dy1-O1	90.04(7)
O4-Dy1-O2	91.58(7)
O4-Dy1-N1	82.88(7)
O4-Dy1-N2	100.72(7)

**Table S5.** Continuous Shape Measures (CShM) values for the potential coordination polyhedra of the 8-coordinate Dy<sup>III</sup> centers in complexes **1-L<sup>N6</sup><sub>phen</sub>** and **1-L<sup>N4O2</sup><sub>phen</sub>**.

Polyhedron <sup>a,b</sup>	<b>1-L<sup>N6</sup><sub>phen</sub></b>	<b>1-L<sup>N4O2</sup><sub>phen</sub></b>
OP	31.58	30.20
HPY	20.42	21.76
<b>HBPY</b>	<b>4.35</b>	<b>1.74</b>
CU	6.72	10.21
SAPR	8.44	16.64
TDD	7.48	14.12
JGBF	5.89	6.41
JETBPY	23.61	23.01
JBTPR	8.04	15.10
BTPR	8.11	14.99
JSD	8.14	15.08
TT	7.56	10.93
ETBPY	21.53	20.38

<sup>a</sup>Abbreviations: OP, Octagon; HPY, Heptagonal pyramid; **HBPY**, Hexagonal bipyramid; CU, Cube; SAPR, Square antiprism; TDD, Triangular dodecahedron; JGBF, Johnson gyrobifastigium; JETBPY, Johnson elongated triangular bipyramid; JBTPR, Biaugmented trigonal prism; BTPR, Biaugmented trigonal prism; JSD, Snub diphenoid; TT, Triakis

tetrahedron; ETBPY, Elongated trigonal bipyramidal. <sup>b</sup> The value in boldface indicates the closest polyhedron according to the Continuous Shape Measures.

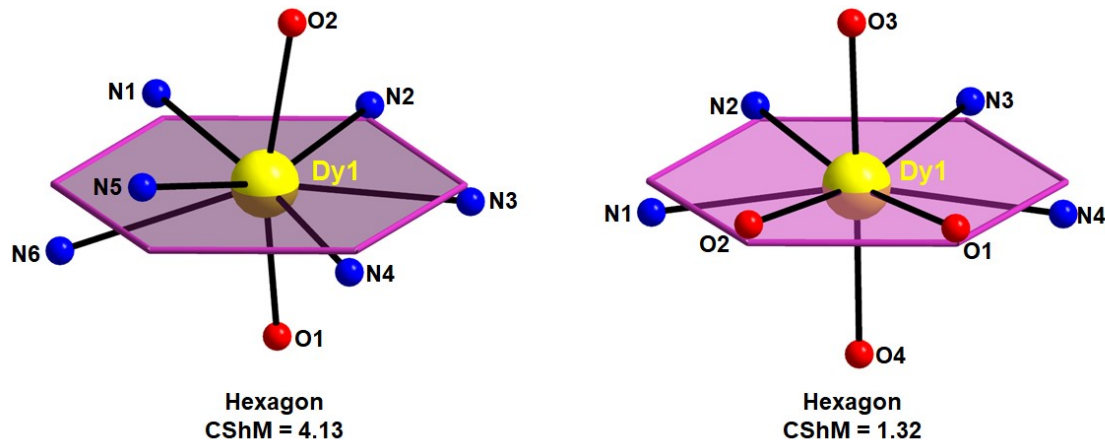


**Fig. S7** Deviation of the equatorial donor atoms of the macrocyclic ligands  $\mathbf{1-L}_{\text{phen}}^{\text{N}6}$  (left) and  $\mathbf{1-L}_{\text{phen}}^{\text{N}4\text{O}2}$  (right) from the ideal hexagonal plane (highlighted with purple color) and the corresponding CShM values derived from the SHAPE program. Color scheme: Dy<sup>III</sup>, yellow; O, red; N, blue.

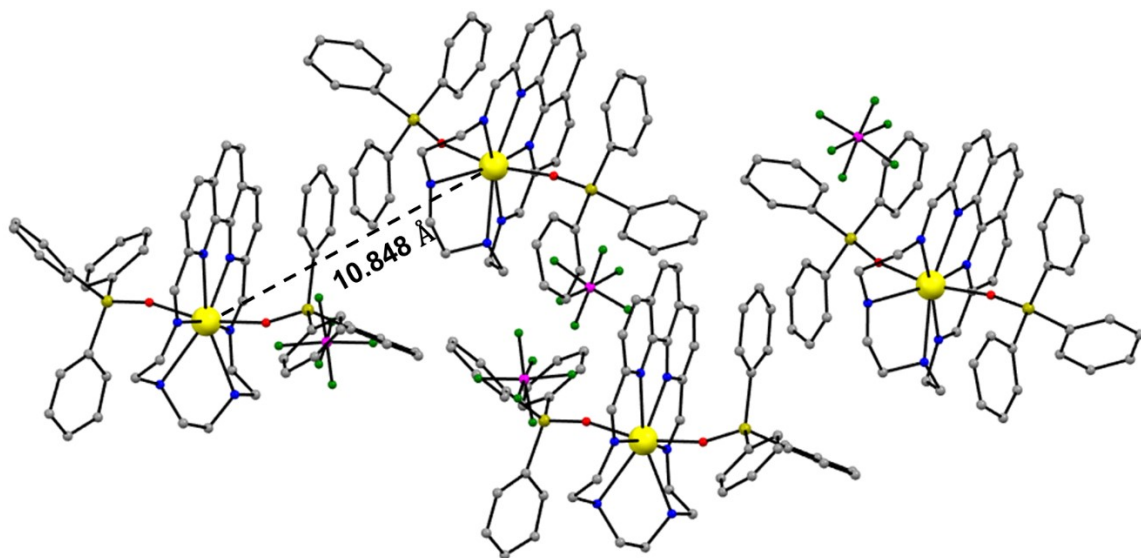


**Fig. S8** A portion of the repeating monomeric complexes in the crystal of  $\mathbf{1-L}_{\text{phen}}^{\text{N}6}$  viewed along the *b*-axis and visualization of the shortest intermolecular Dy...Dy distance as black

dashed lines. Color scheme: Dy<sup>III</sup>, yellow; O, red; N, blue; C, grey; Si, olive; P, magenta; F, dark green. The H-atoms are omitted for clarity.

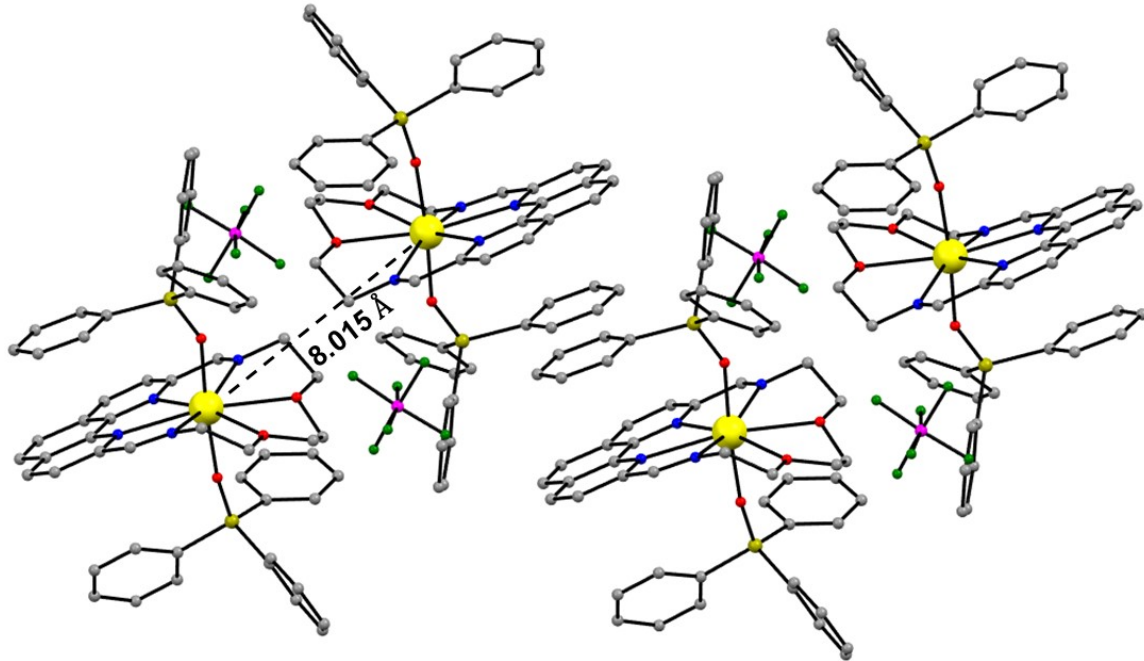


**Fig. S9** A portion of the repeating monomeric complexes in the crystal of **1**-L<sub>phen</sub><sup>N4O2</sup> viewed along the *c*-axis and visualization of the shortest intermolecular Dy···Dy distance as black dashed lines. Color scheme: Dy<sup>III</sup>, yellow; O, red; N, blue; C, grey; Si, olive; P, magenta; F, dark green. The H-atoms are omitted for clarity.

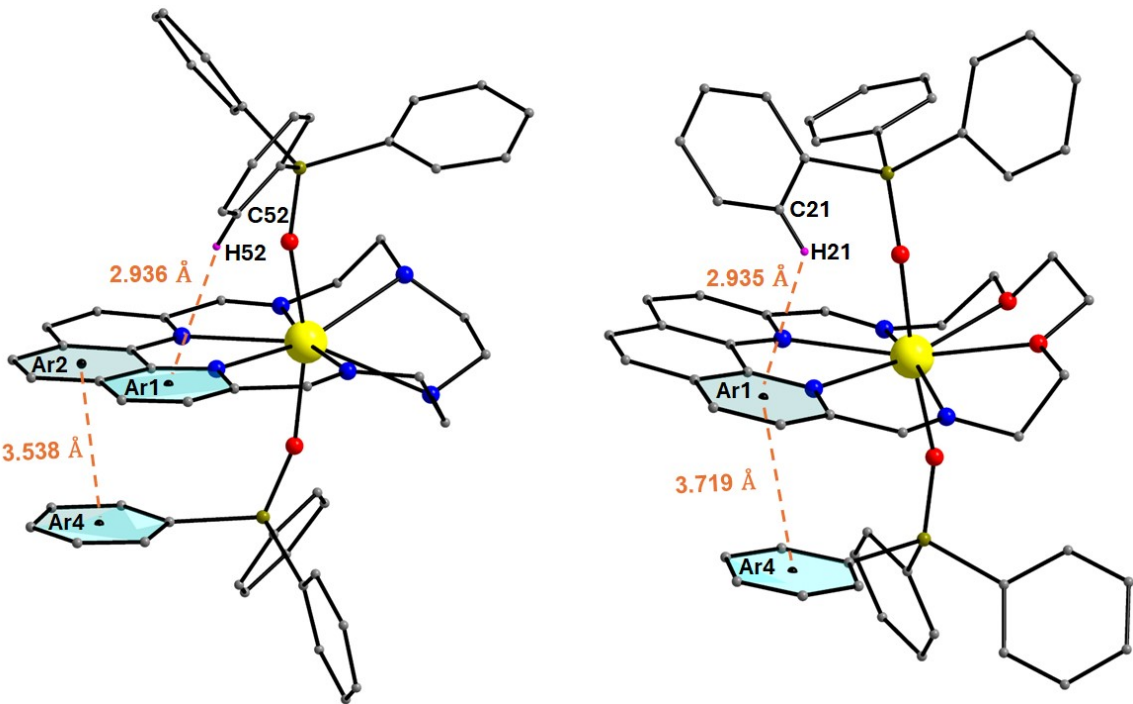


**Fig. S10** Visualization of the intramolecular  $\pi\cdots\pi$  stacking and C-H $\cdots\pi$  interactions as orange dashed lines for compounds  $1-\text{L}_{\text{phen}}^{\text{N}6}$  (left) and  $1-\text{L}_{\text{phen}}^{\text{N}4\text{O}2}$  (right). The aromatic rings (Ar1, Ar2, Ar4) involved in the interactions are highlighted in cyan and the reported distances refer to the corresponding centroids (black spheres of the within the aromatic rings). Color scheme: Dy<sup>III</sup>, yellow; O, red; N, blue; C, grey; Si, olive; H, magenta. Most of the H-atoms are omitted for clarity except for the H-atoms that contribute to the C-H $\cdots\pi$  interactions.

### 3. Magnetic Measurements

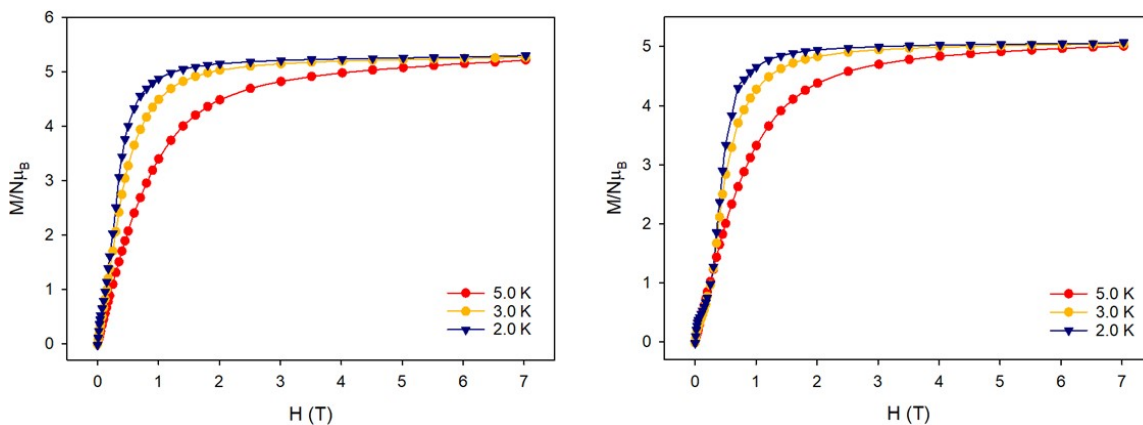


**Fig. S11** Magnetization ( $M$ ) vs field ( $H$ ) plots for complexes  $\mathbf{1}\text{-L}_{\text{phen}}^{\text{N}6}$  (left) and  $\mathbf{1}\text{-L}_{\text{phen}}^{\text{N}4\text{O}2}$  (right) at three different low temperatures. The solid lines are guides only.

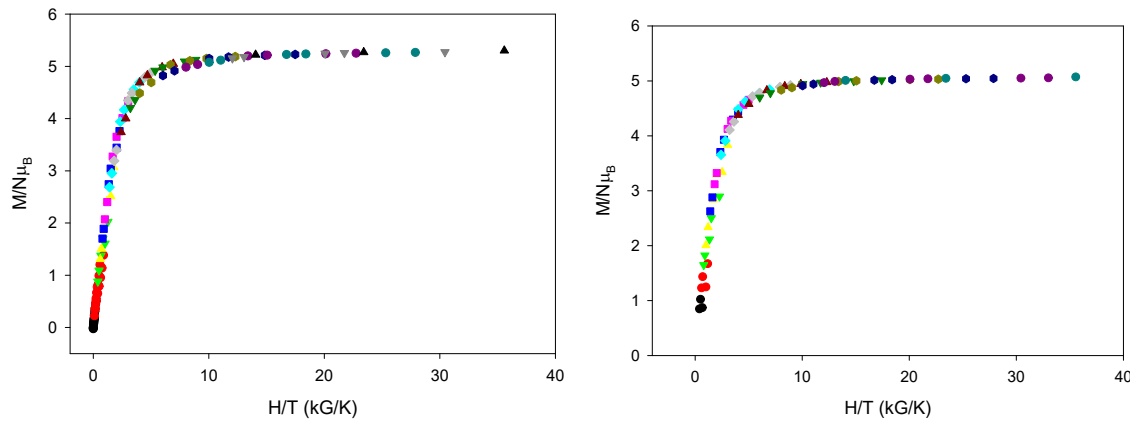


**Fig. S12** Plots of reduced magnetization ( $M/N\mu_{\text{B}}$ ) versus  $H/T$  for  $\mathbf{1}\text{-L}_{\text{phen}}^{\text{N}6}$  (left) and  $\mathbf{1}\text{-L}_{\text{phen}}^{\text{N}4\text{O}2}$  (right) in the temperature range 2-5 K and in different dc fields of 0.05-7.0 T.

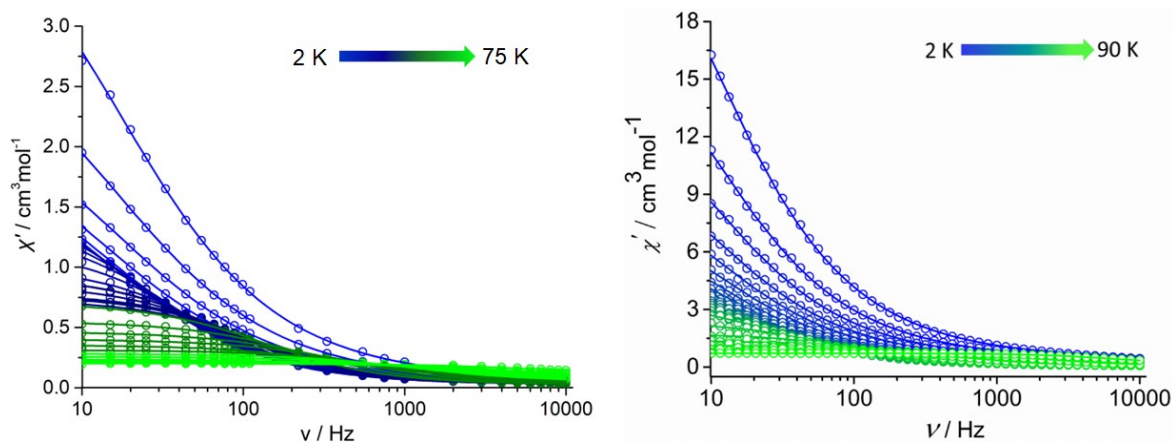


**Fig. S13** (left) Frequency dependence of the in-phase ( $\chi_M'$ ) magnetic susceptibility under zero applied *dc* field for complex  $\mathbf{1}\text{-L}_{\text{phen}}^{\text{N}6}$  over the temperature range 2-75 K. (right) Frequency dependence of the in-phase ( $\chi_M'$ ) magnetic susceptibility under zero applied *dc*

field for complex  $\mathbf{1}\text{-L}_{\text{phen}}^{\text{N}4\text{O}2}$  over the temperature range 2-90 K. Solid lines represent fits to the data.

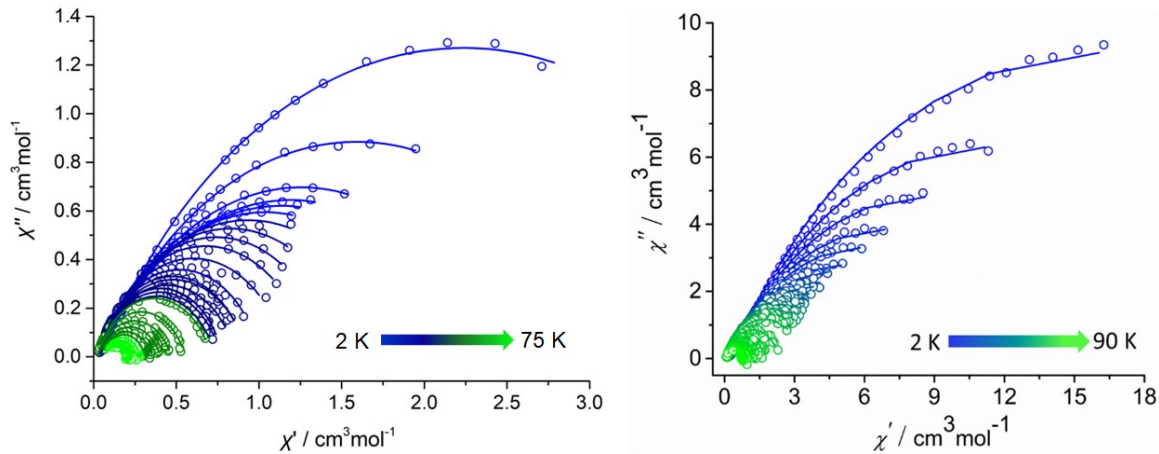


**Fig. S14** (left) Cole-Cole plots for complex  $\mathbf{1}\text{-L}_{\text{phen}}^{\text{N}6}$  obtained from the *ac* susceptibility data in zero applied *dc* field at  $T = 2\text{-}75\text{ K}$ . (right) Cole-Cole plots for complex  $\mathbf{1}\text{-L}_{\text{phen}}^{\text{N}4\text{O}2}$  obtained from the *ac* susceptibility data in zero applied *dc* field at  $T = 2\text{-}90\text{ K}$ . Solid lines represent fits to the data by using **Equations S1** and **S2**.<sup>11</sup> The obtained parameters are reported in **Tables S5** and **S6**.

$$\chi'(\nu) = \chi_{\text{S}} + \frac{(\chi_{\text{T}} - \chi_{\text{S}})[1 + (2\pi\nu\tau)^{(1-\alpha)} \sin(\frac{\alpha\pi}{2})]}{1 + 2(2\pi\nu\tau)^{(1-\alpha)} \sin(\frac{\alpha\pi}{2}) + (2\pi\nu\tau)^{2(1-\alpha)}} \quad (\text{Equation S1})$$

$$\chi''(\nu) = \frac{(\chi_{\text{T}} - \chi_{\text{S}})(2\pi\nu\tau)^{(1-\alpha)} \cos(\frac{\alpha\pi}{2})}{1 + 2(2\pi\nu\tau)^{(1-\alpha)} \sin(\frac{\alpha\pi}{2}) + (2\pi\nu\tau)^{2(1-\alpha)}} \quad (\text{Equation S2})$$

**Table S6.** Relaxation fitting parameters for complex  $\mathbf{1}\text{-L}_{\text{phen}}^{\text{N}6}$ .

$T / \text{K}$	$\chi_{\text{S}} / \text{cm}^3 \text{ mol}^{-1}$	$\chi_{\text{T}} / \text{cm}^3 \text{ mol}^{-1}$	$\tau / \text{s}$	$\alpha$
2	0.05418	4.42245	0.01378	0.32917
3	0.04286	3.13427	0.012905	0.33815

4	0.03883	2.47028	0.012086	0.33673
5	0.03318	2.34429	0.011031	0.35147
6	0.03259	2.22737	0.010068	0.34385
7	0.03401	2.04024	0.009298	0.31818
8	0.03467	1.83133	0.007655	0.28769
9	0.03734	1.61357	0.00664	0.24888
10	0.03812	1.44668	0.005297	0.22343
11	0.03711	1.31751	0.004415	0.21267
12	0.03297	1.16977	0.003552	0.21188
13	0.03148	1.00584	0.002694	0.19212
14	0.02899	0.92446	0.002234	0.18931
15	0.02373	0.93801	0.002157	0.22661
16	0.02277	0.86319	0.001792	0.22100
17	0.02752	0.77971	0.001457	0.18147
18	0.02461	0.76833	0.001383	0.20806
19	0.02240	0.73588	0.001274	0.22255
20	0.02224	0.71020	0.00115	0.22317
25	0.02132	0.55306	0.000673	0.22618
30	0.02280	0.46815	0.000452	0.25184
35	0.03606	0.40417	0.000334	0.24958
40	0.04884	0.34927	0.000258	0.23197
45	0.05313	0.31226	0.000201	0.21884
50	0.05080	0.28250	0.000144	0.23198
55	0.04975	0.25889	9.86E-05	0.27664
60	0.06315	0.23627	7.22E-05	0.28048
65	0.07606	0.21950	5.3E-05	0.27007
70	0.08765	0.20229	3.31E-05	0.20309
75	0.09439	0.20299	1.95E-05	0.22020

**Table S7.** Relaxation fitting parameters for complex **1-L<sup>N4O2</sup><sub>phen</sub>**.

T / K	$\chi_S / \text{cm}^3 \text{ mol}^{-1}$	$\chi_T / \text{cm}^3 \text{ mol}^{-1}$	$\tau / \text{s}$	$\alpha$
2	0.39465	31.75808	0.01594	0.32973
3	0.35161	22.07037	0.01606	0.33088
4	0.31194	16.79102	0.01572	0.32715
5	0.27148	13.48739	0.01596	0.329
6	0.24747	11.53134	0.0164	0.32591
7	0.23048	9.57347	0.01517	0.31629
8	0.20031	9.00968	0.01703	0.32363
9	0.18564	7.77207	0.01513	0.31385
10	0.16981	7.30589	0.01526	0.31193
11	0.17089	6.37683	0.01273	0.28654
12	0.16483	5.75862	0.01089	0.26455
13	0.15736	5.33772	0.00999	0.25542
14	0.15445	4.92041	0.00896	0.23842
15	0.14435	4.44054	0.00772	0.22921
16	0.12357	4.41831	0.00807	0.24544
17	0.12831	4.02777	0.00674	0.22103
18	0.10909	3.93853	0.00683	0.23922
19	0.10279	3.67557	0.00603	0.23061
20	0.11006	3.36029	0.00507	0.20119
30	0.07946	2.35619	0.00248	0.18291
40	0.08572	1.72587	0.00143	0.15188
50	0.09544	1.37284	9.30254E-4	0.13139
60	0.08521	1.13542	5.68139E-4	0.11565
70	0.06895	0.96972	2.86981E-4	0.14617
80	0.04556	0.846	8.83876E-5	0.21352
90	0.1322	0.72005	2.41854E-5	0.14436

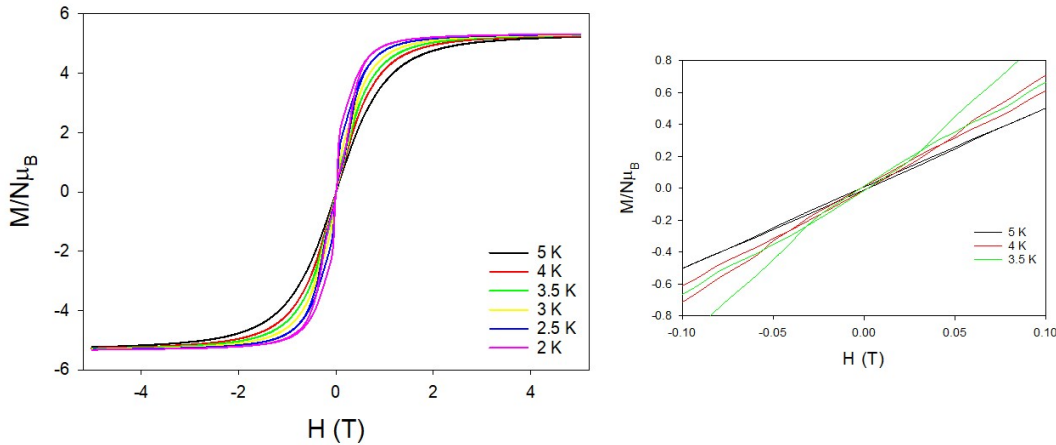


**Fig. S15** Magnetic hysteresis loops for complex  $\mathbf{1-L}_{\text{phen}}^{\text{N}6}$  measured at a temperature range of 2-5 K with a mean field sweep rate of  $40 \text{ Oe s}^{-1}$  (left) and enlargement of the zero-field region from 3.5 to 5 K (right).

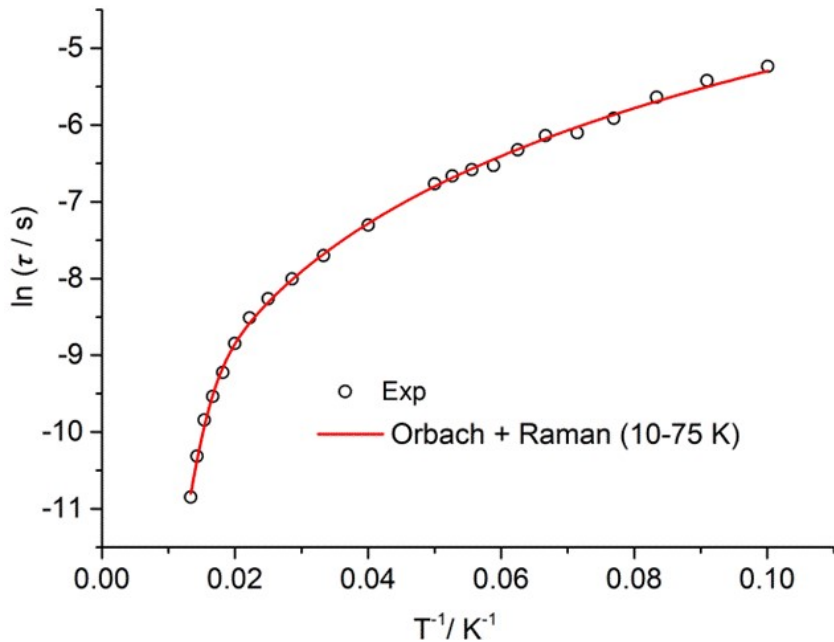


**Fig. S16** Temperature-dependence of relaxation times ( $\tau$ ) for complex  $\mathbf{1-L}_{\text{phen}}^{\text{N}6}$  at the indicated temperature range. The hollow circles correspond to experimental data and the lines to the best-fit of the data using the modified equation:  $\tau^1 = \tau_0^{-1} e^{-U_{\text{eff}}/kT} + CT^n$ , which accounts for the presence of Orbach and Raman processes, respectively. The best-fit parameters were:  $U_{\text{eff}} = 653(27) \text{ K}$ ,  $\tau_0 = 4.97 \times 10^{-9} \text{ s}$ ,  $C = 0.136 (0.026) \text{ s}^{-1} \text{ K}^{-n}$ ,  $n = 2.165 (0.018)$ .

## 4. *Ab initio* Calculations

### Computational Details

All calculations were carried out on the coordinates obtained from the relevant crystal structure using the ORCA 5.0.2 software package.<sup>12</sup> The positions of hydrogen atoms were optimized at the DFT level using a pure GGA PBE exchange correlation functional, keeping the position of the other atoms constant.<sup>13</sup> To avoid the convergence problem, we replaced Dy<sup>3+</sup> with Y<sup>3+</sup> during the optimizations. The def2-TZVP basis sets with effective core potential (ECP) were used to treat the core electrons of yttrium throughout the DFT calculations.<sup>14</sup> In the multi-reference *ab initio* calculations, we used the DKH (Douglas-Kroll-Hess) Hamiltonian throughout to consider relativistic effects. The dysprosium centre was modelled with the SARC2-DKH-QZVP basis set, and all other atoms were treated with the DKH-def2-TZVP basis set in combination with the ‘AutoAux’ auxiliary basis set.<sup>15</sup> The active space CAS(7,9) was constructed from 9 electrons in 7 f-orbitals. In the configuration interaction procedure, 21 sextets, 128 quartets, and 130 doublets were computed for all the complexes. To consider the spin-orbit coupling, we also used the quasi-degenerate perturbation theory (QDPT) approach using SA-CASSCF wave functions.<sup>16</sup> The SINGLE\_ANISO module as implemented in ORCA was used to compute the *g*-tensor and crystal field parameters of the low-lying excited states using previously calculated spin-orbit states.<sup>17</sup>

**Table S8.** *Ab initio* calculated low-lying spin-orbit energy states (in cm<sup>-1</sup>) for the investigated complexes.

1-L <sup>N6</sup> <sub>phen</sub>	1-L <sup>N4O2</sup> <sub>phen</sub>
-----------------------------------	-------------------------------------

0.000	0.000
0.000	0.000
473.4084	512.2405
473.4084	512.2405
848.2715	940.4564
848.2715	940.4564
1060.2955	1188.8054
1060.2955	1188.8054
1122.6255	1243.5533
1122.6255	1243.5533
1144.6168	1307.6070
1144.6168	1307.6070
1219.0120	1381.2880
1219.0120	1381.2880
1289.4793	1478.5084
1289.4793	1478.5084

**Table S9.** Single\_aniso computed energy of the KDs, g, angle between the anisotropic axis of the excited states with the ground state (°), and wavefunctions composition for  $\mathbf{1-L_{phen}^{N6}}$ .

Kramers doublets (KD)	Energy (cm <sup>-1</sup> )	g <sub>x</sub>	g <sub>y</sub>	g <sub>z</sub>	angle (°)	Wave function composition
1	0.000	$3.3 \times 10^{-4}$	$5.7 \times 10^{-4}$	19.85		99.99% ±15/2>
2	473.408	0.1176	0.1195	16.92	0.462	99.4% ±13/2>
3	848.271	0.115	0.342	13.68	1.413	95.9% ±11/2>+3.3% ±1/2>
4	1060.295	2.296	3.576	6.787	69.25	66% ±9/2>+1.7% ±7/2>+0.9% ±5/2>+30.4% ±3/2>+1.0% ±1/2>
5	1122.626	0.829	4.681	10.19	90.39	1.3% ±11/2>+0.5% ±9/2>+1

						$5.5\% \pm 7/2>+27.5\% \pm 5/2>+5$ $.2\% \pm 3/2>+50.0\% \pm 1/2>$
6	1144.617	8.909	6.154	0.558	10.37	$1.7\% \pm 11/2>+8.3\% \pm 9/2>+3$ $2.3\% \pm 7/2>+20.0\% \pm 5/2>+5$ $.2\% \pm 3/2>+32.2\% \pm 1/2>$
7	1219.012	1.053	2.271	10.74	91.59	$0.7\% \pm 11/2>+23.4\% \pm 9/2>+$ $4.1\% \pm 7/2>+4.5\% \pm 5/2>+55$ $.0\% \pm 3/2>+12.4\% \pm 1/2>$
8	1289.479	1.222	5.894	13.39	88.53	$1.5\% \pm 9/2>+46.3\% \pm 7/2>+4$ $6.5\% \pm 5/2>+4.3\% \pm 3/2>+1.$ $0\% \pm 1/2>$

**Table S10.** Single\_aniso computed energy of the KDs, g, angle between the anisotropic axis of the excited states with the ground state ( $^{\circ}$ ), and wavefunctions composition for 1-  
 $L_{phen.}^{N4O2}$ .

Kramers doublets (KD)	Energy (cm $^{-1}$ )	g <sub>x</sub>	g <sub>y</sub>	g <sub>z</sub>	angle ( $^{\circ}$ )	Wave function composition
1	0.000	$6.8 \times 10^{-4}$	$8.0 \times 10^{-4}$	19.87		$99.97\% \pm 15/2>$
2	512.240	0.081	0.089	16.94	0.99	$99.67\% \pm 13/2>$
3	940.456	0.106	0.298	13.77	3.07	$96.47\% \pm 11/2>+2.60\% \pm 1/2>$
4	1188.805	4.169	4.873	7.371	63.40	$55.86\% \pm 9/2>+5.88\% \pm 7/2>+4.83\% \pm 5/2>+29.00\% \pm 3/2>+4.09\% \pm 1/2>$
5	1243.553	1.598	4.694	12.74	93.02	$2.21\% \pm 11/2>+8.91\% \pm 9/2>+2.26\% \pm 7/2>+18.42\% \pm 5/2>+8.22\% \pm 3/2>+59.85\% \pm 1/2>$
6	1307.607	0.934	2.795	10.82	80.85	$0.31\% \pm 11/2>+21.00\% \pm 9/2>+41.10\% \pm 7/2>+22.69\% \pm 1/2>$

						$5/2>+8.09\% \pm 3/2>+4.76\% \pm 1/2>$
7	1381.288	0.535	1.104	15.50	88.27	$0.51\% \pm 11/2>+9.42\% \pm 9/2>+6.69\% \pm 7/2>+12.29\% \pm 5/2>+45.00\% \pm 3/2>+25.96\% \pm 1/2>$
8	1478.508	0.933	2.727	16.22	103.79	$4.41\% \pm 9/2>+41.61\% \pm 7/2>+41.64\% \pm 5/2>+9.60\% \pm 3/2>+2.48\% \pm 1/2>$

**Table S11.** Magnitudes of transition magnetic moment matrix elements (in Bohr magneton) calculated for  $\mathbf{1-L}_{\text{phen}}^{\text{N6}}$ .

Climbing Transition			Crossing Transition		
Initial KD	Final KD	Magnitude	Initial KD	Final KD	Magnitude
1	2	1.770	1	1	$1.5 \times 10^{-4}$
1	3	0.08669	1	2	$6.5 \times 10^{-4}$
1	4	0.05420	1	3	0.01585
1	5	0.04284	1	4	0.02533
1	6	0.03804	1	5	0.02063
1	7	0.05283	1	6	0.02429
1	8	0.02076	1	7	0.02620
2	3	2.381	1	8	0.03927
2	4	0.06380	2	2	0.03953
2	5	0.1360	2	3	0.05910
2	6	0.1658	2	4	0.1150
2	7	0.1489	2	5	0.1904
2	8	0.09861	2	6	0.1417
3	4	2.628	2	7	0.1177
3	5	0.4160	2	8	0.02887
3	6	0.4901	3	3	0.07687
3	7	0.7800	3	4	0.05621

3	8	0.16450	3	5	0.3725
4	5	1.614	3	6	0.7404
4	6	2.027	3	7	0.4313
4	7	1.463	3	8	0.2141
4	8	0.4875	4	4	0.9854
5	6	2.193	4	5	1.737
5	7	1.243	4	6	1.109
5	8	0.8933	4	7	0.8711
6	7	1.354	4	8	0.1912
6	8	0.9205	5	5	2.480
7	8	2.490	5	6	1.184
			5	7	1.132
			5	8	0.4453
			6	6	1.533
			6	7	1.076
			6	8	1.342
			7	7	2.054
			7	8	1.768
			8	8	2.929

**Table S12.** Magnitudes of transition magnetic moment matrix elements (in Bohr magneton) calculated for  $\mathbf{1-L}_{\text{phen}}^{\text{N4O2}}$ .

Climbing Transition			Crossing Transition		
Initial KD	Final KD	Magnitude	Initial KD	Final KD	Magnitude
1	2	1.771	1	1	$2.4 \times 10^{-4}$
1	3	0.04382	1	2	$8.5 \times 10^{-4}$
1	4	0.0329	1	3	0.01187
1	5	0.02467	1	4	0.02681

1	6	0.03593	1	5	0.02641
1	7	0.03240	1	6	0.02016
1	8	0.02520	1	7	0.02938
2	3	2.389	1	8	0.02582
2	4	0.1025	2	2	0.02859
2	5	0.1874	2	3	0.04291
2	6	0.08269	2	4	0.1166
2	7	0.01114	2	5	0.2226
2	8	0.06835	2	6	0.06922
3	4	2.478	2	7	0.1083
3	5	0.8818	2	8	0.04163
3	6	0.8508	3	3	0.07323
3	7	0.5217	3	4	0.2773
3	8	0.2832	3	5	0.6490
4	5	1.647	3	6	0.6727
4	6	2.192	3	7	0.3620
4	7	1.111	3	8	0.1955
4	8	0.4559	4	4	1.834
5	6	1.264	4	5	1.561
5	7	0.9767	4	6	1.889
5	8	0.6181	4	7	0.5669
6	7	1.591	4	8	0.1617
6	8	1.044	5	5	2.751
7	8	1.570	5	6	1.985
			5	7	1.152
			5	8	0.5097
			6	6	1.336

			6	7	0.8251
			6	8	1.703
			7	7	2.820
			7	8	1.7013
			8	8	1.095

**Table S13.** SINGLE\_ANISO computed crystal-field parameters for the studied complexes.

k	q	$\mathbf{1-L}_{\text{phen}}^{\text{N6}}$	$\mathbf{1-L}_{\text{phen}}^{\text{N4O2}}$
	-2	-0.1113E+00	-0.1104E-01
	-1	0.1426E+00	-0.2443E+00
2	0	<b>-0.6786E+01</b>	<b>-0.7773E+01</b>
	1	0.4683E+00	0.1204E+01
	2	-0.3873E+00	0.1453E+01
	-4	-0.1471E-02	-0.1582E-03
	-3	-0.1293E-01	0.4144E-02
	-2	0.1518E-02	-0.1440E-02
	-1	0.6662E-04	0.3319E-02
4	0	<b>-0.1318E-01</b>	<b>-0.1447E-01</b>
	1	-0.6099E-02	-0.9173E-02
	2	0.5784E-02	-0.2907E-02
	3	-0.4535E-01	0.4452E-02
	4	-0.4952E-02	-0.2690E-02
	-6	0.3334E-03	-0.3532E-03
	-5	-0.1649E-03	0.1906E-03

	-4	-0.3472E-05	-0.4379E-05
	-3	-0.4502E-04	0.1024E-04
	-2	0.1561E-04	0.1992E-06
	-1	-0.2039E-04	-0.3355E-04
6	0	<b>0.3971E-04</b>	<b>0.5365E-04</b>
	1	0.5234E-04	0.2397E-04
	2	0.3827E-04	-0.2384E-04
	3	-0.1502E-03	0.1209E-04
	4	-0.2786E-04	-0.3057E-04
	5	-0.2691E-03	0.2181E-03
	6	0.5477E-03	-0.5572E-03

## References

- 1 C.-L. Xiao, C.-Z. Wang, L.-Y. Yuan, B. Li, H. He, S. Wang, Y.-L. Zhao, Z.-F. Chai and W.-Q. Shi, *Inorg. Chem.*, 2014, **53**, 1712–1720.
- 2 G. A. Bain, J. F. Berry, *J. Chem. Ed.* 2008, **85**, 532-536.
- 3 P. Loeffen, Oxford Diffraction. *CrysAlis CCD and CrysAlis RED*. Oxford Diffraction Ltd.: Abingdon, UK: Oxford Diffraction. CrysAlis CCD and CrysAlis RED, 2008.
- 4 A. Altomare, G. Cascarano, C. Giacovazzo, A. Guagliardi, M. C. Burla, G. Polidori, M. Camalli, *J. Appl. Crystallogr.* 1994, **27**, 435.
- 5 G. M. Sheldrick, *SHELXS-97 and SHELXL-97, Program for Crystal Structure Solution and Refinement*, University of Gottingen, Gottingen, 1997.
- 6 G. M. Sheldrick, *Acta Cryst C*, 2015, **71**, 3–8.
- 7 D. Oxford, *CrysAlis CCD and CrysAlis RED, version 1.71*. Oxford Diffraction, Oxford, England, 2007.
- 8 L. J. Farrugia, *J. Appl. CrystallogR.* 1999, **32**, 837-838.
- 9 C. F. Macrae, P. R. Edgington, P. McCabe, E. Pidcock, G. P. Shields, R. Taylor, M. Towler, J. V. D. Streek, *J. Appl. Crystallogr.* 2006, **39**, 453-457.
- 10 K. Brandenburg, H. Putz, *DIAMOND, Release 3.1f*, Crystal Impact GbR. Bonn, Germany, 2006.
- 11 K. S. Cole and R. H. Cole, *J. Chem. Phys.*, 1941, **9**, 341–351.

- 12 F. Neese, F. Wennmohs, U. Becker and C. Riplinger, *J. Chem. Phys.*, 2020, **152**, 224108.
- 13 (a) J. P. Perdew, K. Burke and M. Ernzerhof, *Phys. Rev. Lett.*, 1997, **78**, 1396-1396.  
(b) J. P. Perdew, K. Burke and M. Ernzerhof, *Phys. Rev. Lett.*, 1996, **77**, 3865-3868.
- 14 (a) A. Schäfer, H. Horn and R. Ahlrichs, *J. Chem. Phys.*, 1992, **97**, 2571-2577. (b) F. Weigend and R. Ahlrichs, *Phys. Chem. Chem. Phys.*, 2005, **7**, 3297-3305.
- 15 (a) D. Aravena, F. Neese and D. A. Pantazis, *J. Chem. Theory Comput.*, 2016, **12**, 1148-1156. (b) J. Chmela and M. E. Harding, *Mol. Phys.*, 2018, **116**, 1523-1538.
- 16 D. Ganyushin and F. Neese, *J. Chem. Phys.*, 2006, **125**, 024103.
- 17 L. F. Chibotaru and L. Ungur, *J. Chem. Phys.*, 2012, **137**, 064112.